REGULARIZED SAR TOMOGRAPHY APPROACHES

Alessandra Budillon[1]*, Loïc Denis*[2]*, Clément Rambour*[4]*, Gilda Schirinzi*[1]*, Florence Tupin*[3]

[1]Dipartimento di Ingegneria, Università degli Studi di Napoli "Parthenope"
Centro Direzionale di Napoli, Isola C/4, 80143 Napoli, Italy
[2]UJM-Saint-Etienne, CNRS, Institut d Optique Graduate School
Laboratoire Hubert Curien UMR 5516, F-42023, SAINT-ETIENNE, France
[3]LTCI, Télécom Paris, Institut Polytechnique de Paris, France
[4]CEDRIC (EA4629), Conservatoire National des Arts et Métiers, HESAM Université, 75003 Paris

ABSTRACT

Synthetic Aperture Radar (SAR) tomographic techniques enable the reconstruction of the scene scattering structure along the vertical direction and can provide the temporal evolution of a cloud of reliable points located in the 3D space. The use of Generalized Likelihood Ratio Test approaches have been shown to be effective in selecting reliable multiple scatterers. Recently regularized tomographic methods have been proposed for increasing the density of the recovered scatterers in urban environments. This paper discusses the differences between these two approaches and performs a comparison of reconstruction results obtained from a stack of TerraSAR-X images, in a region of interest located in the city of Paris, France.

Index Terms— SAR Interferometry, SAR Tomography, Differential Tomography, Scatterers detection, GLRT, regularized inversion

1. INTRODUCTION

Synthetic Aperture Radar (SAR) Tomographic techniques (TomoSAR) exploit multi-pass acquisitions for generating 3-D reflectivity profiles of the imaged scene. They exploit the amplitude and phase of the received data and offer the possibility to resolve multiple scatterers [1, 2, 3, 4], lying in the same range–azimuth resolution cell. In urban environment this issue is very important since layover causes multiple coherent scatterers to be mapped to the same range-azimuth image pixel. Due to the small number of acquisitions available and/or uneven distribution of the baselines, TomoSAR techniques suffer from the presence of ambiguities and high sidelobe level in the reconstructed height-reflectivity profiles.

TomoSAR techniques proved to be an excellent tool for reconstruction and monitoring of urban areas, since in this case they can benefit from the sparsity property of the reflectivity profile along the elevation direction, which allows the use of super-resolution techniques based on compressive sensing (CS) [3, 4]. These techniques, besides to improve height resolution, allow to reduce the number of acquisitions. However, they suffer of the presence of outliers and high sidelobes in the reconstructed profile that can heavily affect the reconstruction accuracy. To solve this problem, different methods based on the use of statistical hypothesis tests have been introduced [5, 6]. In [6, 7] the discrimination between reliable scatterers and outliers (false alarms) has been addressed based on a Generalized Likelihood Ratio Test (GLRT) denoted as Fast-Sup-GLRT. This statistical test is based on the search of the signal support (i.e. the positions of the significant samples in the unknown reflectivity sparse vector) that best matches the data and non-linear maximization for detecting the scatterers with an assigned probability of false alarm and estimating their elevation. The result of the GLRT based tomographic processing is given as a cloud of reliable point scatterers with known intensity and appropriately located on the ground structures. Their possible millimetric temporal and/or thermal displacements can be also estimated [7, 8]. A reconstruction of the continuous surface describing the structures on the ground (f.i. buildings, roads, bridges, etc.) is possible only when the spatial density of the points in the cloud is sufficiently high.

In applications related to urban areas, to improve the tomographic reconstruction accuracy and increase the point cloud density, the peculiar geometry and the presence of vertical and horizontal planes can be exploited. Buildings are structured objects with generally straight vertical walls and flat rooftops. Using these geometrical priors on the scatterers distribution may strongly decrease the number of outliers in the reconstructions but requires performing the tomographic reconstruction for several pixels at once. Approaches constraining the estimated reflectivity to account for some geometrical priors present higher robustness to outliers than conventional CS [9], whereas post-processing methods can retrieve structured information such as buildings shapes, footprints or surfaces [10, 11, 12, 13]. In this paper the approaches presented in [6] and [13], are investigated through a qualitative

and quantitative analysis on real data.

2. METHODOLOGY

Starting from N coregistered images, SAR tomography aims at retrieving the 3-D reflectivity function of a scene. An estimate of the 3-D reflectivity function can be found by inverting for each pixel the forward model:

$$\mathbf{v} = \mathbf{A}(\mathbf{h})\,\mathbf{u} + \epsilon, \tag{1}$$

where $\mathbf{v}$ is the SAR data vector (i.e. the collection of N single-look complex values at a given range-azimuth resolution cell), $\mathbf{u}$ is the reflectivity vector, $\boldsymbol{\epsilon}$ represents the noise, $\mathbf{h}$ collects the N_h heights along the elevation axis and the $N \times N_h$ sensing matrix $\mathbf{A}(\mathbf{h}) = \left[\mathbf{a}(h_1) \cdots \mathbf{a}(h_{N_h})\right]$ is obtained by the concatenation of the so-called steering vectors: the i-th column of $\mathbf{A}(\mathbf{h})$ is defined by

$$\begin{aligned}\mathbf{a}(h_i) &= \left[\exp(-j\xi_1 h_i) \cdots \exp(-j\xi_N h_i)\right]^{\mathrm{T}} \\ &= \exp(-j\boldsymbol{\xi} h_i)\,,\end{aligned} \tag{2}$$

where $\boldsymbol{\xi} \in \mathbb{R}^N$ collects the N angular frequencies ξ_1 to ξ_N (angular frequencies are related to the spatial frequencies through $\xi_n = 4\pi b_n/(\lambda R_0)$, with b_n the perpendicular baseline, R_0 the distance between the image pixel and the reference antenna position, and λ the operating wavelength). Tomography consists in inverting equation (1), *ie.*, retrieving $\mathbf{u}$ given $\mathbf{v}$, at each pixel.

We describe in the following paragraphs two different strategies to perform this inversion and identify meaningful scatterers on the urban surfaces.

2.1. Detection based on Fast-Sup-GLRT

This method assumes that at most K_{max} scatterers with different elevations are present in each ramge-azimuth resolution cell. In order to detect the scatterers and to estimate their elevation and reflectivity, a Generalized Likelihood Ratio Test (GLRT) approach is used. The general detection problem is formulated in terms of $K_{max}+1$ statistical hypotheses. If, for instance, the presence of at most two scatterers ($K_{max} = 2$) has to be detected, the following three statistical hypothesis applies: $\{H_0$: absence of scatterers, H_1: presence of a single scatterer and H_2: presence of a double scatterer$\}$. The test is performed sequentially: first a decision between the hypothesis H_0 and H_1 is performed, then, if H_0 is decided the test stops while if H_1 is decided, a second step is applied for deciding between H_1 and H_2. For the details and the expression of the test, see [6]. At each step, the Ratio Test is compared with a threshold derived through Monte Carlo simulation and following a CFAR (Constant False Alarm Rate) approach, fixing a probability of false alarm.

2.2. Regularized inversion with smoothness priors

In contrast to the previous approach that performs an extraction of meaningful scatterers, we now consider reconstructing the spatial distribution of reflectivity. Given the ill-posed nature of the inverse problem of estimating reflectivities $\boldsymbol{u}_{\square}$ in 3D, given a stack of observed SLC SAR images $\boldsymbol{v}_{\square}$, regularization terms are mandatory. The 3D volume of reflectivities is estimated by solving the following minimization problem[14]:

$$\hat{\boldsymbol{u}}_{\square} = \underset{\boldsymbol{u}_{\square}}{\arg\min}\ \frac{1}{2}||\boldsymbol{\Phi}\,\boldsymbol{u}_{\square} - \boldsymbol{v}_{\square}||_2^2 + \mathscr{R}(|\boldsymbol{u}_{\square}|)\,, \tag{3}$$

where $\mathscr{R}$ is a regularization term that applies only on the modulus of the complex reflectivities. In urban areas, scatterers located on man-made structures (ground, building facades, roofs) form the dominant contribution to the SAR signal. A natural regularization is to favor solutions $\hat{\boldsymbol{u}}_{\square}$ with a small number of scatterers: $\mathscr{R}(|\boldsymbol{u}_{\square}|)$ then corresponds to the ℓ_0 pseudo-norm, or to the ℓ_1 norm. Such sparsity-promoting is referred to as compressive sensing [4]. The linear operator $\boldsymbol{\Phi}$ in (3) projects a 3D volume of reflectivities to a stack of SAR images. Under the approximation that lines orthogonal to the radar line-of-sight are each mapped to a different pixel in the SAR images, the optimization problem (3) can be solved independently for each line. To enforce spatial smoothness in the 3D reconstruction, i.e., to favor volumes where neighboring voxels have similar reflectivity values, other regularization terms can be considered such as the squared ℓ_2 norm of the spatial gradient: $\mathscr{R}(|\boldsymbol{u}_{\square}|) = \mu \sum_i \|\boldsymbol{\nabla}_i |\boldsymbol{u}_{\square}|\|_2^2$, where $\boldsymbol{\nabla}_i |\boldsymbol{u}_{\square}| \in \mathbb{R}^3$ is the spatial gradient of the modulus of the reflectivity at pixel i. Due to the coupling of the unknowns of the problem, minimization problem (3) has to be solved jointly for all voxels of $\boldsymbol{u}_{\square}$. A possible strategy to perform the optimization is the Alternating Directions Method of Multipliers (ADMM) and its variants [9].

3. EXPERIMENTAL RESULTS

We compare these two approaches on a stack of 40 TerraSAR-X spotlight images acquired over the front de Seine in the south-west of Paris, France. The slant-range resolution is 0.45 m and the azimuth resolution is 0.87 m. The total spatial baseline is more than 775 m, and the total temporal baseline is more than 5 years. The theoretical resolution in height is around 6.6 m. Reconstruction results are shown in Fig 1. In Fig. 1 (a) the 3D point clouds obtained with [6], with $K_{max} = 2$ and fixing the probability of false alarm equal to 10^{-3}, are reported, and in (b) the surface reconstructions obtained without spatial regularization (only a sparsity constraint) and with the regularized approach [13] are shown. It can be noted that the regularized approach benefits of an evident spatial smoothing.

In order to perform a quantitative comparison of the scatterer extraction technique Fast-Sup-GLRT and the regularized volumic reconstruction, we used the completeness and accuracy metrics first introduced in [15]. Table 1 illustrates how these two metrics are defined: the completeness characterizes the density of the reconstructed 3D cloud by computing the average distance between each visible element of the ground truth surface and its closest neighbor in the reconstructed cloud. The denser the reconstructed cloud, the smaller this average distance. The accuracy defines how accurate the reconstructed points are. It corresponds to the mean distance to the true surface: the parameter is large when reconstructed points are far from the actual surface. In Table 1, we report this accuracy for both algorithms and for various densities of the reconstructed point cloud, as characterized by the completeness values (from dense reconstructions with a completeness of 1m to sparse reconstructions with elements of the ground truth surface on average 10m away from the closest reconstructed point). This density sampling is obtained by using different probabilities of false alarm for the Fast-Sup-GLRT method while, for the regularized inversion, it corresponds to a local maxima extraction after a thresholding of the reflectivity. Three regimes can be distinguished in Table 1. First, for dense point clouds, the scatterers extraction algorithm Fast-Sup-GLRT reaches a lower reconstruction error. Then, for point clouds presenting a trade-off between accuracy and completeness the regularized inversion tends to present a lower error. Finally, for sparser point clouds, both approaches lead to very similar scores with a slightly lower error for the Fast-Sup-GLRT algorithm. Fast-Sup-GLRT, by controlling the maximum number of scatterers within each resolution cell reduces the risk of mistaking a sidelobe for a scatterer, explaining the first regime. The regularized inversion allows to reduce the non-structured outliers intensity allowing to obtain both a low error and a complete representation in the second regime. Finally, as the representation becomes sparser, only the strongest scatterers are kept and almost no outliers are present in the point clouds.

4. CONCLUSION

In this paper a qualitative and quantitative analysis on real data of two different tomographic techniques, a GLRT approach [6] and a regularized approach [13], has been conducted. In particular completeness and accuracy metrics [15] have been considered, that measure how dense and how accurate the tomographic reconstruction is. Both approaches have been designed in order to select the more reliable points, the GLRT [6] uses thresholds based on a CFAR approach, while [13] includes spatial information in the regularized inversion approach. These two approaches present a complementary behavior : the Fast-Sup-GLRT approach exhibits a high robustness in dense point clouds while the inclusion of spatial information allows to achieve a slightly better accuracy-completeness trade-off. Approaches combining both strategies may then be promising for SAR tomography over urban areas.

	completeness (m) completeness measures the average distance from the ground truth surface to reconstructed points: low value ← denser reconstruction → large value					
	1.0	1.5	2.9	5.4	7.0	10.2
	mean distance to true surface (m) coarse reconstruction = large mean distance accurate reconstruction = low mean distance					
algorithm:						
Fast-Sup-GLRT	**5.1**	**4.9**	3.2	2.7	**2.0**	**1.9**
Regularized inversion	6.6	5.9	**2.9**	**2.5**	2.1	2.1

Table 1. Quantitative evaluation of 3D points reconstructed by SAR tomography. The table reports the localization error for each algorithm, as a function of the density of the reconstructed point cloud, as characterized by the completeness values.

5. REFERENCES

[1] A. Reigber and A. Moreira, "First demonstration of airborne SAR tomography using multibaseline L-band data," *IEEE Transactions on Geoscience and Remote Sensing*, vol. 38, no. 5, pp. 2142–2152, Sep. 2000.

[2] G. Fornaro, F. Lombardini, and F. Serafino, "Three-dimensional multipass SAR focusing: experiments with long-term spaceborne data," *IEEE Transactions on Geoscience and Remote Sensing*, vol. 43, no. 4, pp. 702–714, April 2005.

[3] A. Budillon, A. Evangelista, and G. Schirinzi, "Three-Dimensional SAR Focusing From Multipass Signals Using Compressive Sampling," *Geoscience and Remote Sensing, IEEE Transactions on*, vol. 49, pp. 488 – 499, 02 2011.

[4] X. X. Zhu and R. Bamler, "Super-Resolution Power and Robustness of Compressive Sensing for Spectral Estimation With Application to Spaceborne Tomographic SAR," *IEEE Transactions on Geoscience and Remote Sensing*, vol. 50, no. 1, pp. 247–258, Jan 2012.

[5] G. Fornaro, F. Lombardini, A. Pauciullo, D. Reale, and F. Viviani, "Tomographic processing of interferometric sar data: Developments, applications, and future research perspectives," *IEEE Signal Processing Magazine*, vol. 31, no. 4, pp. 41–50, July 2014.

[6] A. Budillon, A. C. Johnsy, and G. Schirinzi, "A Fast Support Detector for Superresolution Localization of

Multiple Scatterers in SAR Tomography," *IEEE Journal of Selected Topics in Applied Earth Observations and Remote Sensing*, vol. 10, no. 6, pp. 2768–2779, June 2017.

[7] A. Budillon, A. Johnsy, and G. Schirinzi, "Extension of a fast GLRT algorithm to 5D SAR tomography of Urban areas," *Remote Sensing*, vol. 9, pp. 844, 08 2017.

[8] A Budillon, M Crosetto, Angel Johnsy, O Monserrat, Vrinda Krishnakumar, and Gilda Schirinzi, "Comparison of Persistent Scatterer Interferometry and SAR Tomography Using Sentinel-1 in Urban Environment," *Remote Sensing*, vol. 10, 12 2018.

[9] C. Rambour, L. Denis, F. Tupin, and H. M. Oriot, "Introducing Spatial Regularization in SAR Tomography Reconstruction," *IEEE Transactions on Geoscience and Remote Sensing*, pp. 1–18, 2019.

[10] X. X. Zhu and M. Shahzad, "Facade reconstruction using multiview spaceborne tomoSAR point clouds," *IEEE Transactions on Geoscience and Remote Sensing*, vol. 52, no. 6, pp. 3541–3552, June 2014.

[11] M. Shahzad and X. Zhu, "Reconstruction of Building Footprints Using Spaceborne TomoSAR Point Clouds," *ISPRS Annals of Photogrammetry, Remote Sensing and Spatial Information Sciences*, vol. II-3/W5, pp. 385–392, 08 2015.

[12] A. Ley, O. D'Hondt, and O. Hellwich, "Regularization and Completion of TomoSAR Point Clouds in a Projected Height Map Domain," *IEEE Journal of Selected Topics in Applied Earth Observations and Remote Sensing*, vol. 11, no. 6, pp. 2104–2114, June 2018.

[13] C. Rambour, L. Denis, F. Tupin, H. Oriot, Y. Huang, and L. Ferro-Famil, "Urban surface reconstruction in SAR tomography by graph-cuts," *Computer Vision and Image Understanding*, vol. 188, pp. 102791, 2019.

[14] C. Rambour, A. Budillon, A. C. Johnsy, L. Denis, F. Tupin, and G. Schirinzi, "From Interferometric to Tomographic SAR: A review of synthetic aperture radar tomography-processing techniques for scatterer unmixing in urban areas," *IEEE Geoscience and Remote Sensing Magazine*, vol. to appear, 2020.

[15] O. D'Hondt, C. López-Martínez, S. Guillaso, and O. Hellwich, "Nonlocal filtering applied to 3-d reconstruction of tomographic sar data," *IEEE Transactions on Geoscience and Remote Sensing*, vol. 56, no. 1, pp. 272–285, Jan 2018.

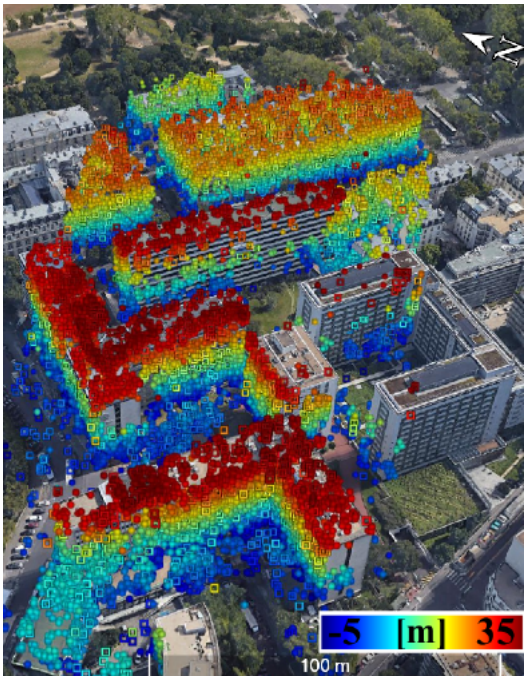

(a) 3D point clouds

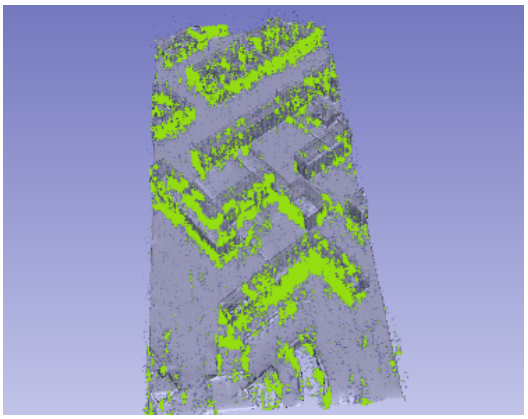

(b) Estimated reflectivity under sparse and smooth priors

Fig. 1. Results on real data using (a) the Fast-Sup-GLRT algorithm and (b) the regularized inversion